LAWRENCE
LIVERMORE
NATIONAL
LABORATORY

LLNL-CONF-579617

Brute Force Modeling of the Kessler Syndrome

S. Nikolaev, D. Phillion, H. K. Springer, W. deVries, M. Jiang, A. Pertica, J. Henderson, M. Horsley, S. Olivier

September 10, 2012

AMOS
Kihei, Maui, HI, United States
September 11, 2012 through September 14, 2012

Disclaimer

This document was prepared as an account of work sponsored by an agency of the United States government. Neither the United States government nor Lawrence Livermore National Security, LLC, nor any of their employees makes any warranty, expressed or implied, or assumes any legal liability or responsibility for the accuracy, completeness, or usefulness of any information, apparatus, product, or process disclosed, or represents that its use would not infringe privately owned rights. Reference herein to any specific commercial product, process, or service by trade name, trademark, manufacturer, or otherwise does not necessarily constitute or imply its endorsement, recommendation, or favoring by the United States government or Lawrence Livermore National Security, LLC. The views and opinions of authors expressed herein do not necessarily state or reflect those of the United States government or Lawrence Livermore National Security, LLC, and shall not be used for advertising or product endorsement purposes.

BRUTE FORCE MODELING OF THE KESSLER SYNDROME

Sergei Nikolaev, Donald Phillion, H. Keo Springer, Willem deVries,
Ming Jiang, Alex Pertica, John Henderson, Matthew Horsley, Scot Olivier
Lawrence Livermore National Laboratory

ABSTRACT

The Kessler Syndrome (runaway increase in the number of orbiting objects through cascading collisions) presents a serious danger to future space missions. To understand its implications and study the effectiveness of various debris mitigations strategies, we developed a state-of-the-art evolutionary model for the near-Earth environment using the brute force computational approach. The model propagates and monitors every object in orbit at high temporal resolution for the length of simulation (100+ years). To meet the demand of the required computational power, the model is implemented as a parallel computer code on LLNL's high-performance supercomputers. Here we describe the details of the model and present the results of the simulations.

1. INTRODUCTION

The near-Earth space environment currently includes more than 15,000 man-made objects greater than 10cm in size, including dead and operational spacecraft, rocket stages, and various pieces of "space junk": satellite break-up fragments, mission-related debris, Al_2O_3 slag, NaK coolant droplets, etc. While the atmospheric drag force gradually removes the objects in low-Earth orbit (LEO) through reentries, the overall number of orbiting objects keeps growing due to continuing launch activity, spontaneous on-orbit breakups and space collisions. The increasing crowding in LEO was highlighted by the 2009 Cosmos-Iridium collision.

The increased density of objects in near-Earth environment increases the likelihood of the catastrophic collisions involving space assets, and as a consequence, the risk to both manned and unmanned space programs. As of now, a typical object in LEO experiences several close (<10 km) conjunctions per day, with each conjunction having a small but finite probability of becoming a collision. Once a collision occurs, the resulting debris cloud expands into orbital space, increasing the probability of future collisions. When the density of orbiting objects is sufficiently high, the collisions may become self-sustaining, potentially becoming a runaway process. This self-sustaining "collisional cascading" problem, also known as the Kessler syndrome, has been recognized since the 1970's [2]. Recent studies have concluded that the existing debris environment in altitudes between 700 km and 1000 km is already unstable [3].

Given the importance of the problem, numerous models have been built both to characterize the debris environment [4-7] and to study its long-term evolution [8-10]. Historically, all evolutionary models of near-Earth space environment have relied on a semi-analytical approach and space object density approximations to calculate the collision probabilities. One exception is the NASA's latest evolutionary debris model, LEGEND [10,11], which studies the future growth of the debris environment by propagating every catalog object. Although probably the most sophisticated model to-date, LEGEND model has a limited time resolution: the conjunctions/collisions are evaluated on a timescale of 5-15 days, potentially missing the effects on a shorter time scale, e.g. critical early evolution of debris cloud, potential collisions involving re-entering objects, etc. This limitation is a *necessity:* running LEGEND at finer time resolutions would increase the run times considerably.

Here, we present a new evolutionary model of near-Earth environment, which overcomes the deficiency of the LEGEND model. The model numerically keeps track of every object in space (greater than 10 cm in size) for the length of the simulation (100+ years) with *high temporal resolution*. Nominally, the time step in our model is dt=22.5 sec (a factor of ~20,000 better than LEGEND's), but in reality the temporal resolution is much finer, since our positions are quadratically interpolated. The initial population of objects is taken from the actual USSTRATCOM TLE catalog as of May 2009. Each object in the initial set is assigned a realistic mass and size from observed distributions, according to its classification (payload, rocket stage, or debris fragment). The initial population is then allowed to evolve, with additions due to new launches, spontaneous breakups, and collisions, and subtractions due to the atmospheric reentries. The propagation is done by a custom written, efficient orbital

propagator that takes into account the atmospheric drag force. During the simulation, each object is continuously tracked and all its close conjunctions are evaluated (we always use full N×N conjunctions evaluations). The propagator positions are treated as the actual positions with no errors. Each conjunction is resolved into collision or non-collision using the ratio of combined sizes to the closest approach distance. For each realized collision, we generate new debris fragments using NASA's Standard Breakup Model [12] and update the catalog of the orbiting objects to include the newly formed debris fragments. The new objects will then be tracked for the length of the simulation along with the original objects. Given the statistical nature of the model (random satellite parameters, uncertainties in projected solar activity, etc.), it requires a large number of independent runs to calculate the expected outcome and characterize the uncertainties. Due to the high amount of the computing power required to run the model, we utilized several high-capacity supercomputers at LLNL.

All events occurring during the simulation are logged to disk, allowing studying the distribution of conjunction parameters (e.g. location, relative velocities, closest approach distance, etc.), finding cascade collisions, and evaluating collision risk to specific assets. In addition, the full orbiting object catalog is periodically dumped to disk for verification and visualization purposes.

The applications of the model are numerous. In this work, we focus on the long-term evolution of the near-Earth orbital environment, studying the effects of different future launch activities and orbital breakup rates on the debris population in space. In addition, the model can be used for shorter projected time intervals (e.g. 10-20 years into the future) to evaluate the on-orbit collision risk for specific assets over their planned mission time, e.g. ISS, IRIDIUM, IRIDIUM NEXT, etc. This application space could be of particular interest to space insurance industry. Another potential use of the model includes evaluation of the proposed active debris removal strategies. For example, the model enables conducting detailed trade-off studies comparing the effects of removal of few large debris pieces vs. many smaller ones.

2. THE MODEL

The following sections describe the model components. The start date of the simulation is May 4th, 2009 (MJD=54955.0), with the starting TLE-based catalog including 12971 objects. The lower limit on the object size in the model is 10 cm. The size limit applies to debris generation: when modeling debris clouds from on-orbit breakups or collisions, we only keep track of fragments greater than 10 cm. Depending on a scenario and hardware configuration, a typical run covers 100-150 simulation years. Every object in the simulation has a spherical geometry, for ease of resolving conjunctions into collisions.

2.1. Objects Size and Mass Distribution

Using proper size and mass distributions for orbiting objects is critical to ensure the unbiased frequency of collisions (determined by the object size) and the average lifetime in orbit (determined by the object's area-to-mass ratio, or AMR). In the absence of the actual data for most orbiting objects, we use the distributions derived from the actual data (limited sample) to assign sizes and masses to orbiting objects. The distributions are derived by analyzing payload masses listed in NSSDC database [13], as well as the mass spectrum of debris fragments from NASA Standard Breakup Model.

To assign a mass to the orbiting object in a catalog, we use the classification in TLE catalog (payload, debris, or rocket body) and sample the mass from a lognormal distribution depending on the type of the object:

$$\begin{cases} \lg m \propto N(3.0, 0.5) & \text{spacecraft and rocket stages} \\ \lg m \propto N(-1.2, 0.6) & \text{debris fragments} \end{cases} \quad (1)$$

The debris mass distribution is derived by examining debris with characteristic size d>10 cm from two 3m objects colliding at 5 km/sec. For the initial population of spacecraft and rocket stages, we adopt the limits $1.0 < \lg m < 4.0$. For payloads whose mass is available in the literature, we use the actual mass values instead of the randomly sampled ones. Once the mass is assigned, the effective cross-section of the object is obtained from:

$$\begin{cases} \lg A = 0.80 \lg m - 1.8, \ \sigma = 0.3 & \text{spacecraft and rocket stages} \\ \lg A = 0.85 \lg m - 0.8, \ \sigma = 0.8 - 0.1(\lg m + 4) & \text{debris fragments} \end{cases} \quad (2)$$

The randomly drawn values are subject to constraints, -2.0 < lg A for satellites and rocket bodies, and -2.2586 < lg A for debris fragments. Given the relationship between the effective area and the characteristic size in the NASA Standard Breakup Model, $A = 0.556945 d^{2.0047077}$, the relation between the mass and the diameter is $\lg m = 2.51 \lg d + 1.93$.

2.2. Orbital Propagator and Effects of the Atmosphere

Given the critical role of the atmospheric drag in removing objects from LEO, and the extended length of the simulation (100+ years), the simplified B* treatment of existing SGP4 propagator [14] is not adequate. Instead, we designed our own specialized propagator, called Simplified Analytic Propagator (SAP).

The Simplified Analytic Propagator uses the well-known equations for the nodal and apsidal precession rates due to J_2 obtained using Laplace's Variation Of Parameters (VOP) method [15], including the time derivative of the mean anomaly:

$$\begin{cases} \dot{\Omega} = -\frac{3}{2} \frac{1}{(1-e^2)^2} n J_2 \left(\frac{R}{a}\right)^2 \cos i \\ \dot{\omega} = \frac{3}{4} \frac{1}{(1-e^2)^2} n J_2 \left(\frac{R}{a}\right)^2 \left(5\cos^2 i - 1\right) \\ \dot{M} - n = \frac{3}{4} \frac{1}{(1-e^2)^{3/2}} n J_2 \left(\frac{R}{a}\right)^2 \left(3\cos^2 i - 1\right) \end{cases} \quad (3)$$

It also includes the contributions of the Sun and Moon third body perturbations to these precessions using Kozai's treatment [16], with only the secular terms linear in t included.

Compared to SGP4 propagator, SAP is faster and has more sophisticated modeling of the atmospheric drag. In this work, we mainly use the Jacchia-Bowman 2008 atmospheric model [17], but other models (e.g. NRL MSISE-00, GOST2004, Jacchia-Roberts 1971, etc.) can be incorporated just as easily. For GEO orbital regime, where the atmospheric drag is negligible, the SAP is nominally less accurate than SGP4, since it models only J_2 and Sun and Moon perturbations. In practice, however, very little accuracy is lost, since the magnitude of the J_2 coefficient is several hundred times greater than all the other coefficients combined. To verify that the accuracy is acceptable, we have compared the SAP with SGP4 for different types of orbits with no drag (B* made zero in the TLE). The osculating Keplerian elements at various times show that the nodal and apsidal precessions are almost identical.

The secular terms due to the atmospheric drag are computed using the Jacchia-Bowman 2008 (JB2008) model and the actual solar weather files. The contribution to the first time derivatives, $\dot{a}$, $\dot{e}$, $\dot{i}$, $\dot{\Omega}$, $\dot{\omega}$, and the first and second time derivatives of the mean anomaly, $\dot{M}$, $\ddot{M}$, are computed by averaging over one orbit. The publically available JB2008 FORTRAN code was rewritten in C++ for easier integration and verified against the original code. With the simulated runs extending more than 100 years into the future, the projected solar activity is one of the major sources of uncertainty in the model. In our simulation, we use the last full 11-year cycle for which complete solar weather information is available and repeat the cycle in the model assuming an exact 11-year periodicity. To introduce variations to the solar weather model, we randomly perturb the state of the atmosphere by randomizing the sampling time within a 14-day window.

The SAP atmospheric drag model was verified by comparing the predicted atmospheric reentry time of the UARS satellite with its actual reentry time. Given the satellite mass, m=5900 kg, and the effective cross-section area A_e=50 m^2, and using the NORAD TLE for UARS for July 22, 2008 epoch, the UARS reentry was predicted for

August 21, 2011. The actual reentry occurred September 24, 2011, giving the uncertainty of 2.9%. Given the large number of unknowns, this accuracy is acceptable. In addition, the atmospheric drag model was verified by comparing the computed orbital decay rates for the ISS with the observations.

2.3. Simulation Events

Having assigned mass, size, and type value to each of the 12971 initial objects in orbit (TLE catalog from May 4th, 2009), the simulation proceeds by propagating each of the objects for each time step. At the beginning of each time interval, the atmospheric state is updated. The effect of the random number generator seed value is to perturb the state of the atmosphere from the canonical value from JB2008 value. In each time interval, the model allows for the following effects: new launches, on-orbit collisions, spontaneous breakups, and atmospheric reentries.

The launch rate and the payload number distribution are derived from historic data [18]. As the representative of the recent launch activity, we used 8-year time interval from 2001 to 2009. In the specified interval, there were 513 launches (860 payloads), which gives the average launch rate λ_{launch}=0.1736 day^{-1}. Despite existing monthly and day-of-month variations in the launch rates, those were not modeled. The launch activity is modeled by a simple Poisson process with the rate λ, with the number of payloads sampled from the distribution in Table 1.

TABLE 1. The distribution of the number of payloads per launch based on historic data, 2001-2009.

Payloads per Launch	Actual Frequency	Modeled Frequency	Payloads per Launch	Actual Frequency	Modeled Frequency
1	352	352	11	0	0.3
2	92	92	12	0	0.3
3	36	36	13	0	0.3
4	11	11	14	1	0.3
5	5	7	15	0	0.3
6	5	5	16	0	0.1
7	2	3	17	0	0.1
8	2	2	18	1	0.1
9	5	2	19	0	0.1
10	1	1	20	0	0.1

The element set for each new launch is sampled from the same historic dataset. To avoid redundancy in the element sets, we perturb the Keplerian elements slightly from their original values, by adding a normally distributed offsets with σ_a = 10km, σ_e = 0.001, σ_i = 1°. The orbital elements Ω and ω were drawn uniformly from [0, 2π].

The spontaneous on-orbit breakups are also modeled by a simple Poisson process with a rate $\lambda_{breakup}$=0.0123 day^{-1}. The rate was derived from historic on-orbit breakup data. By early 2007, there have been ~200 spontaneous on-orbit breakup events [19]. The model includes the much lower probability of a break-up for GEO objects (historically, there have been only 2 breakup events at GEO [20]), by adopting the extra 0.01 factor for the GEO breakup rate. Furthermore, with the expected stricter adherence to end-of-life disposal (post-mission reentries, or re-orbiting) and passivation measures (controlled fuel/pressurant venting, depletion burns, batteries discharge, etc), the breakup rate is projected to decline in future. In the model, we experimented with the linear decrease in the breakup rate by an order of magnitude, $\lambda_{breakup}$=0.00123 day^{-1} in 100 or 200 years. In the event of a break-up, the debris cloud is modeled by the NASA Breakup Model. Briefly, the model uses a set of empirically derived distributions calibrated to match the observed debris clouds from actual breakup and collision events. It quantifies the distributions of debris sizes, AMR, effective cross-section areas A, and the imparted velocities of the debris fragments, while making a distinction between debris from spacecraft and rocket bodies. As a result of a break-up event, the original object is removed from the catalog and replaced by the set of fragments, generated by the break-up debris model.

The reentries are monitored at every time interval, by simply comparing the expected reentry time for each object (calculated by the propagator) with the current time: when the latter exceeds the former, the object is removed from the catalog.

The on-orbit collisions are modeled by monitoring all close (100 m or less) approaches (conjunctions) among the orbiting objects. During the length of the simulation, the parameters (coordinates, closest approach distance, relative velocity, types of conjuncting objects, etc) of every close conjunction are recorded. Over a hundred simulation years, this gives a very large database of conjunction parameters, ideally suited to study future risks to orbiting objects. To speed up the conjunction analysis, we pre-screen the object pairs by examining the perigee and apogee of each orbit (the ranges have to overlap for the conjunction to be possible). The conjunctions are calculated on the interpolated propagated positions, effectively at infinitesimal time resolution. Rather than assuming a collision probability as a function of approach distance, we employ a simple geometric argument: when the combined radii of the conjuncting objects are greater than the closest approach distance, the conjunction is turned into a collision. Effectively, this treatment assumes that the propagator gives the absolute truth in terms of the objects positions, with zero-size uncertainty ellipsoid. While seemingly idealistic, our approach is in fact unbiased with respect to the collision probability, since all of the effects contributing to the uncertaintly ellispoid are modeled through inherent randomness of the Monte-Carlo method. Once a collision occurs, the debris generation model is triggered to create the debris clouds. We have developed our own debris generation model, based on extensive hydrocode computer modeling of satellite collisions for various engagement conditions, relative velocities, object materials, etc. For this work, however, we use NASA Standard Breakup Model, to facilitate the comparison of the results to other semi-analytic models (e.g. LEGEND) using the same debris generator.

2.4. Numerical Implementation

The simulation requires a significant allocation of computing power (>10 million CPU-hours), which is the main reason such a simulation has not been implemented before. Our two typical "production" run configurations use 8192 CPUs for 64 hours (525K CPU-hours) or 15408 CPUs for 16 hours (246K CPU-hours). Smaller runs are done using 4128 CPUs for 16 hours (66K CPU-hours). To take full advantage of the large-capacity computing hardware at LLNL, the model is implemented as an MPI-parallel code. Specifically, the model employs a dual parallelization schema: the simulation time interval is split among the CPU "pools", while the CPUs in pools each work on a subset of the object catalog (Fig. 1). This results in a very flexible setup allowing us to run the simulation on a variety of CPU allocations and wall-clock time limits. Typically, each CPU pool works on ~90-min simulated time interval.

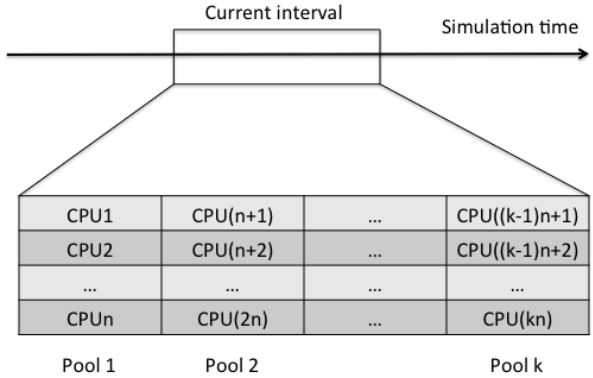

Fig. 1. Parallelization schema, splitting the time interval among the CPU pools (columns), and splitting the object catalog among the CPUs within the pool (rows).

The number of CPU pools is chosen such that the total length of the simulation time interval is 7-10 days, as the larger time intervals would increase the error due to solar activity model. Each computing core maintains its own copy of the orbiting object catalog. All catalog-changing events (launches, reentries, breakups, collisions) are synchronized among the cores. The most time-consuming part of the simulation is the conjunction analysis, which needs to evaluate the close approaches among N objects. Naively, this operation is $O(N^2)$, although we optimize it by careful screening of objects according to their orbital regimes (e.g. a GEO object at 36000 km will never approach a LEO object at 500 km). If several CPUs report a collision during the same simulation time interval, the earliest collision is effected, triggering debris generation and catalog update and synchronization among the CPUs. The simulation clock is then reset to the collision time, and the model resumes the execution from the latest collision time.

3. RESULTS

Fig. 2 shows the evolution of the population of orbiting objects as a function of time, for a number of distinct scenarios:

- BAU, "business as usual" launch/breakup activity: maintains the current (2009) rates for new launches and on-orbit breakups;
- BAU-d, "business as usual with decreasing breakup rate": same as BAU except the on-orbit breakup rate is linearly decreasing by a factor of 10 over 200 years;
- NL, "no launches": zero new launch rate and constant (2009) on-orbit breakup rate;
- NB, "no breakups": zero breakup rate, constant (2009) new launches rate;
- NFL, "no future launches": new launch rate is set to zero, while breakup rate is linearly decreasing by a factor of 10 over 100 years;
- NLNB, "no launches, no breakups": both rates are set to zero.

The NFL scenario was chosen to compare the results of the runs to LEGEND model, which has a similar scenario. The figure shows several interesting traits. The initial dip in the number of objects, common to all scenarios, is in part real, due to Sun becoming more active, and in part artificial due to some LEO objects being assigned too high

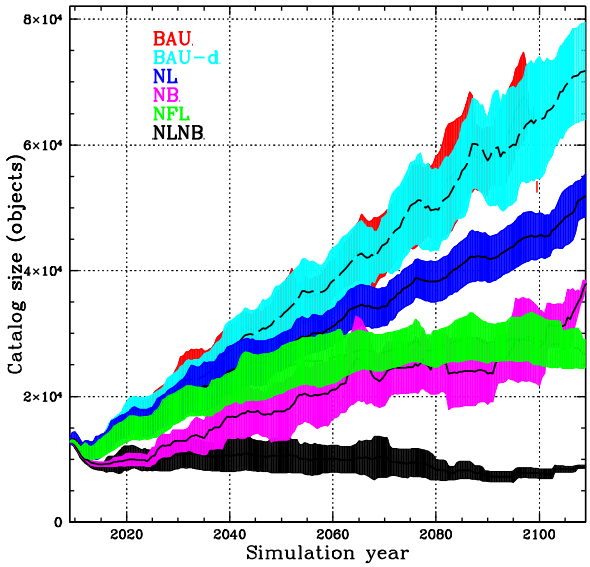

Fig. 2. Evolution of the number of orbiting objects with time, averaged over multiple runs. The shaded regions indicate 1-sigma limits. The decreasing sigma range beyond year 2080 in some scenarios is due to fewer runs reaching these simulation times.

AMRs. The most pessimistic scenarios (BAU and BAU-d) are virtually identical, and result is linear growth of the catalog size with time, to ~65,000 objects by year 2100. Even in the most optimistic NLNB scenario, the total number of orbiting objects stays roughly constant at ~10,000 throughout the length of the simulation runs, with the collisional debris fragments compensating the natural removal of objects through atmospheric reentries. The average uncertainty of the estimates is at the level of 10-30% for all scenarios. The main conclusions from Fig. 3 are 1) that one needs a complex approach to space debris problem, combining diminished future launch activity, measures to prevent on-orbit breakups, and likely some form of active debris removal; and 2) that even in the most optimistic case, it will take some time before the results are seen and felt.

Tables 2 and 3 summarize the conjunction/collision statistics for BAU and NLNB scenarios, averaged over multiple runs. The statistics are calculated for 10-year simulation time bins, and show the relative fractions of collisions and conjunctions by objects types. The number of collisions in each bin is normalized by the number of runs actually covering the bin. For the number of collisions, we scale the actual number of collisions per decade by the fraction of the decade covered by the simulation.

TABLE 2. The relative numbers of conjunctions and collisions for BAU scenario, averaged over multiple runs, by objects types: intact-intact (i-i), intact-fragment (i-f), fragment-fragment (f-f).

Simulation time, yrs	Number of conjunctions/day				Number of collisions/year			
	i-i	i-f	f-f	total	i-i	i-f	f-f	total
0-10	0.24	0.82	1.24	2.30	0.03	0.07	0.00	0.10
10-20	0.29	1.31	2.30	3.90	0.08	0.16	0.00	0.23
20-30	0.34	2.09	4.99	7.41	0.17	0.26	0.00	0.42
30-40	0.40	2.82	7.18	10.40	0.09	0.30	0.02	0.41
40-50	0.48	3.55	10.16	14.18	0.12	0.54	0.03	0.70
50-60	0.54	4.36	13.19	18.09	0.21	0.34	0.03	0.58
60-70	0.63	5.30	17.26	23.19	0.24	0.53	0.03	0.79
70-80	0.70	6.71	25.49	32.90	0.31	0.93	0.13	1.37
80-90	0.76	6.95	26.80	34.51	0.23	0.98	0.05	1.26
90-100	0.91	9.75	39.25	49.91	1.00	2.00	0.00	3.00

In both scenarios, the conjunction rate is dominated by fragment-on-fragment conjunctions, while the collision numbers show the predominance of intact-on-fragment collisions. This is due to the much higher effective cross-section of the intact objects, compared to debris fragments.

TABLE 3. Same as Table 2, but for NLNB scenario.

Simulation time, yrs	Number of conjunctions/day				Number of collisions/year			
	i-i	i-f	f-f	total	i-i	i-f	f-f	total
0-10	0.20	0.54	0.69	1.44	0.04	0.02	0.00	0.07
10-20	0.19	0.49	0.85	1.53	0.12	0.04	0.00	0.17
20-30	0.18	0.58	0.86	1.62	0.02	0.07	0.00	0.09
30-40	0.17	0.52	0.75	1.44	0.02	0.01	0.00	0.03
40-50	0.17	0.49	0.69	1.35	0.01	0.07	0.01	0.10
50-60	0.17	0.47	1.45	2.09	0.10	0.03	0.00	0.12
60-70	0.16	0.57	1.16	1.89	0.01	0.12	0.01	0.15
70-80	0.16	0.42	0.64	1.21	0.03	0.02	0.00	0.05

The atmospheric reentries rate is shown in Fig. 3. The rate displays an 11-year solar activity cycle (active Sun heats the atmosphere, which causes it to swell and increase the drag on the orbiting objects, causing them to reenter).

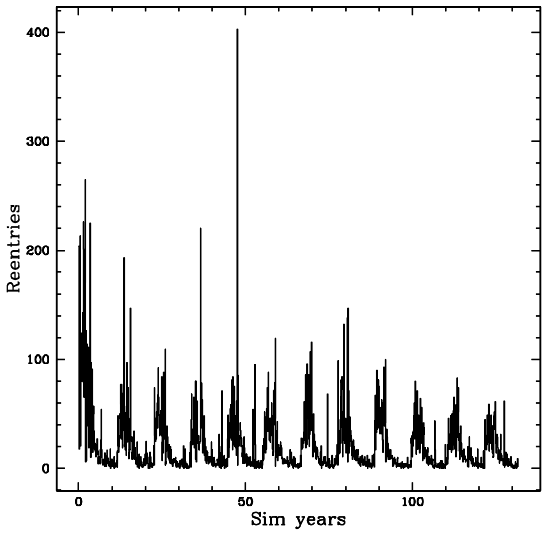

Fig. 3. The monthly rate of atmospheric reentries for a typical model run, showing 11-year cycle of solar activity.

The conjunction dataset accumulated over the simulation length offers incredibly detailed look into the distributions of conjunction parameters. We obtain high- resolution data on the distribution of conjunction velocities, approach angles, altitudes, latitudes, etc. Fig. 4 shows the location of all close conjunctions in LEO. The concentric circles seen in the distribution of conjunctions as viewed from a pole indicate regions of elevated conjunction rate (risk) due to clustering in altitude-elevation parameter space.

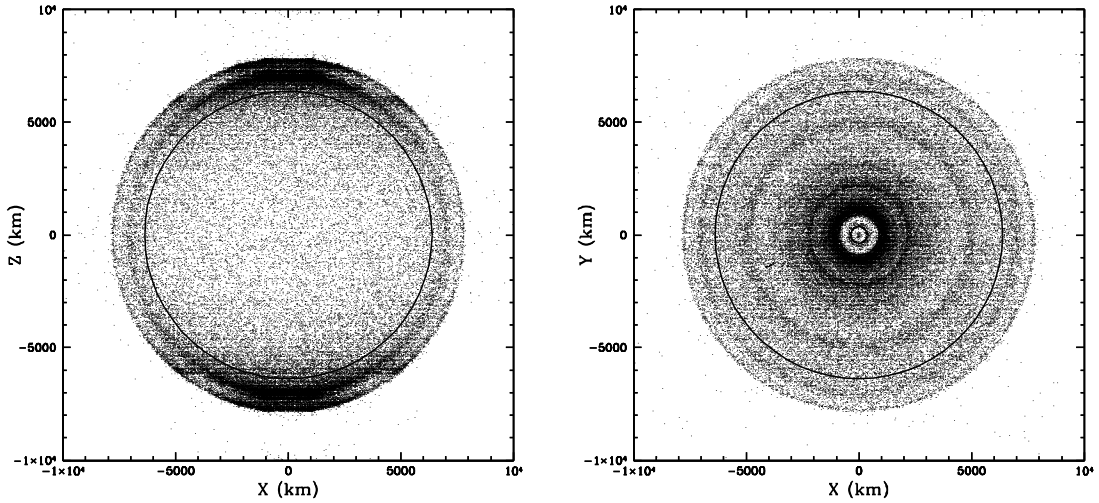

Fig. 4. Conjunction locations in ECI coordinates (X,Y,Z). Solid circle indicates Earth surface.

To demonstrate how the model can be used to evaluate collision risk for space assets, we studied the conjunction history for the International Space Station (ID #25544). With the parameters assigned to the ISS in the simulation, m = 450,000 kg, A = 550m^2, the station would reenter the atmosphere within the first five years of simulation, unless some altitude-maintaining procedure were implemented. To mimic the orbit-boosting burns, we implemented a simple approach where the altitude of ISS is instantaneously boosted to 400km as soon as it drops below 350km. Fig. 5 shows the altitude profile of ISS during one particular run (under BAU-d scenario) and the cumulative conjunction rate projected to 2030.

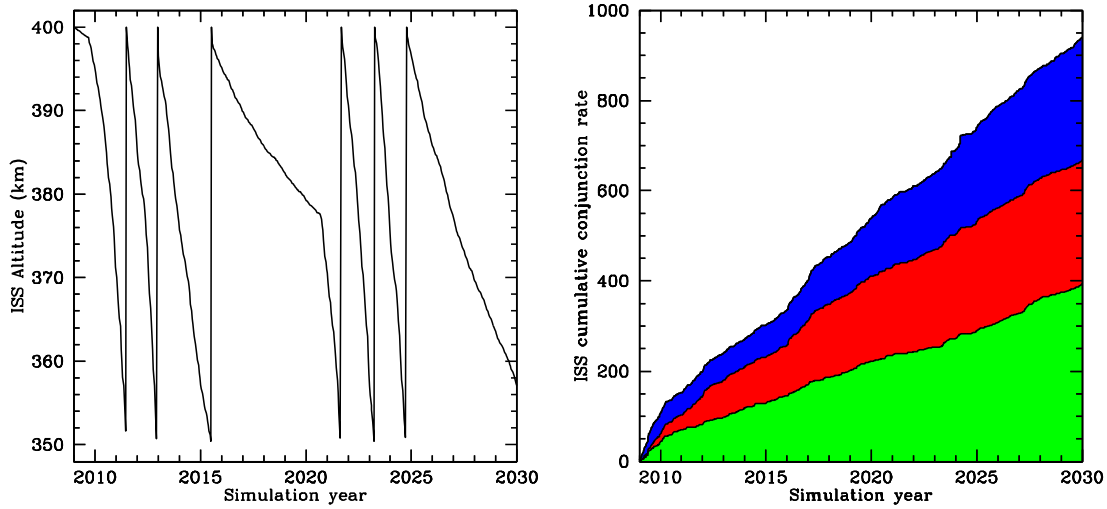

Fig. 5. *Left:* Evolution of the ISS altitude in the simulation; *Right:* ISS cumulative conjunction rate (100m conjunctions) as a function of time. Contributions to total rate from payloads (green), rocket bodies (red), and debris fragments (blue) are shown. Note the correlation of the orbital decay rate with the solar activity phase.

Fig. 6 shows the evolution of the conjunction rate for various scenarios, averaged over multiple runs. The contributions according to the object types (intact-intact, intact-fragment, fragment-fragment) are shown. The

strongest contributions to the conjunction rate are from fragment-fragment conjunctions, due to the debris fragments being the most numerous of all orbiting objects. For the worst-case scenario (BAU), the number of these very close, 100m conjunctions per day can reach 50 by the year 2100. By comparison, the intact-intact conjunction rate is relatively small, less than one such conjunction per day, even in the worst-case scenario.

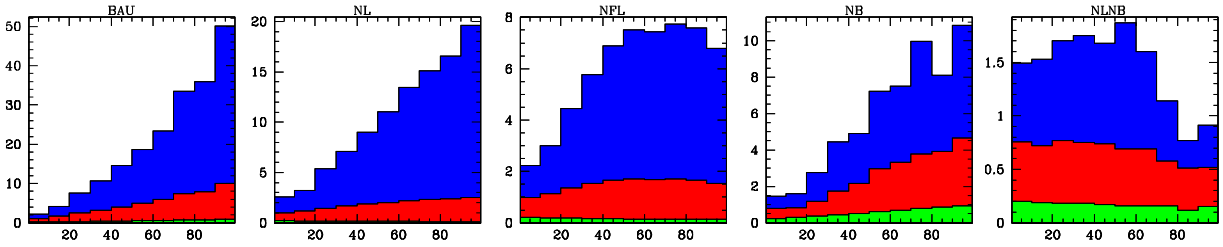

Fig. 6. Conjunction rates (100m conjunctions per day) for five launch/breakup scenarios, BAU, NL, NFL, NB, NLNB (left to right). Shown are the contributions to the total rate from intact-intact (green), intact-fragment (red), and fragment-fragment (blue) conjunctions. The abscissa is simulation years.

Fig. 7 shows the collision rate for different scenarios, again showing individual contributions to the total rate. As for conjunctions, the rates are averaged over multiple scenario runs. Contrary to the Fig. 6, the collision rate is dominated by the intact-intact and intact-fragment collisions. This is due to the much larger cross-section area of the intact objects compared to the debris fragments.

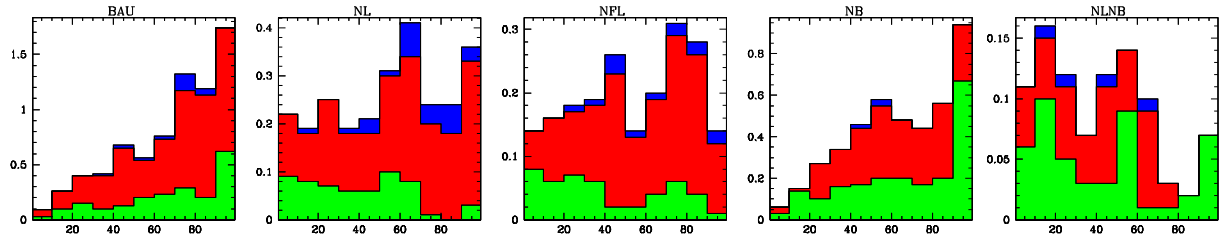

Fig. 7. The evolution of the collision rate (collisions per decade) with time, for BAU, NL, NFL, NB, NLNB scenarios (left to right). The colors indicate the contributions to the total rate from intact-intact collisions (green), intact-fragment collisions (red), and fragment-fragment collisions (blue). The abscissa is simulation years.

4. SUMMARY

The implemented model pushes the state-of-the-art in evolutionary debris modeling by tracking the entire population of orbiting objects (down to 10 cm in size), at high temporal resolution, for the entire length of the simulation. The major source and sink functions are modeled, including new launches, on-orbit breakups, collisions, and atmospheric reentries. The specially developed propagator ensures accurate evolution of the objects in LEO, where the atmospheric effect is critical. A fast conjunction analysis code continuously finds the conjunctions among objects in the simulation, resolving collisions based on the ratio of the combined object sizes to the approach distance. The main objective for designing the model is to study the timescale of the Kessler syndrome timescale, i.e. when cascading collisions become dominant source of debris in space. In addition, the model will help study the efficiency of various policies affecting debris mitigation in space. Finally, the model can be used to predict the collision risk for any particular object in space (e.g. ISS).

Acknowledgments

This work performed under the auspices of the U.S. Department of Energy by Lawrence Livermore National Laboratory under Contract DE-AC52-07NA27344. The authors wish to thank Nicholas Johnson (NASA JSC) for many insightful comments and invaluable suggestions to improve the model, as well as for the supporting data on orbiting objects masses and dimensions. Time allocation on Livermore Computing's (LC) high-performance computing resources was provided under the Multiprogrammatic and Institutional Computing Initiative and through the Grand Computing Challenge (FY2012) allocation. The authors wish to thank Brian Carnes, Greg Tomaschke, Dave Dannenberg, Ryan Day, and LC operators and run coordinators for their support of the large-scale computer

simulations for this work. The IM release number for the document is LLNL-CONF-579617.

References

1. NASA Safety Standard NSS 1740.14, *Guidelines and Assessment Procedures for Limiting Orbital Debris*, 1995
2. D. J. Kessler, B. G. Cour-Palais, *Journal of Geophysical Research* 83, 63 (1978)
3. D. J. Kessler, P. D. Anz-Meador, *Critical Number of Spacecraft in Low Earth Orbit: Using Satellite Fragmentation Data to Evaluate the Stability of the Orbital Debris Environment*, JSC #28949 and LMSEAT #33303 (2000)
4. D. J. Kessler, et al., *A Computer-Based Orbital Debris Environment Model for Spacecraft Design and Observation in Low Earth Orbit*, NASA TM-104825 (1996)
5. J.-C. Liou, M. J. Matney, P. D. Anz-Meador, D. J. Kessler, *The New NASA Orbital Debris Engineering Model ORDEM2000*, NASA/TP—2002-210780 (2002)
6. H. Sdunnus, et al., "The ESA MASTER'99 space debris and meteoroid reference model", Proceedings of the 3rd European Space Debris Conference, ESA SP-473 (2001)
7. M. Oswald, P. Wegener, S. Stabroth, et al., "The MASTER 2005 Model", Proc. of the 4th European Conf. on Space Debris. ESA, 235-242 (2005)
8. P. H. Krisko, R. C. Reynolds, A. Bade, et al., *EVOLVE 4.0 User's Guide and Handbook*, Lockheed Martin Space Operations Report LMSMSS-33020, Houston, TX (2000)
9. L. Anselmo, A. Cordelli, R. Jehn, et al., "New results of the upgraded SDM space debris modeling software", IAA.99-6.5.08. 50th Intl. Astronautical Congress, Amsterdam, The Netherlands (1999)
10. J.-C. Liou, et al., *Advances in Space Research*, 34, 981-986 (2004)
11. J.-C. Liou, *Advances in Space Research*, 38, 2102-2106 (2006)
12. N. L. Johnson, et al., *Advances in Space Research*, 28, 1377-1384 (2001)
13. http://nssdc.gsfc.nasa.gov
14. F. R. Hoots, R. L. Roehrich, "Spacetrack Report No. 3: Models For Propagation of NORAD Element Sets", Adc/Do6 (Peterson AFB: Project Spacetrack Reports, Office of Astrodynamics, Aerospace Defense Center) (1980)
15. M. Capderou, *Satellites Orbits and Missions*, Springer-Verlag (2005)
16. Y. Kozai, "On the effects of the sun and moon upon the motion of a close earth satellite", Smithsonian Astronomical Observatory Special Report #22, part 2 (1959)
17. B. R. Bowman, *A New Empirical Thermospheric Density Model JB2008 Using New Solar and Geomagnetic Indices*, AIAA/AAS Astrodynamics Specialist Conference, 18-21 August 2008, Honolulu, Hawaii
18. http://www.planet4589.org
19. N. L. Johnson, et al., *History of On-Orbit Satellite Fragmentations*, 14th ed., NASA/TM-2008- 214779, Lyndon B. Johnson Space Center (2008)
20. N. L. Johnson, "Evidence for historical satellite fragmentations in and near the geosynchronous regime", Proc. of the Third European Conference on Space Debris, 19 - 21 March 2001, Darmstadt, Germany. Ed.: Huguette Sawaya-Lacoste. ESA SP-473, Vol. 1, Noordwijk, Netherlands: ESA Publications Division, ISBN 92-9092-733-X, 2001, p. 355 - 359 (2001)